JACS
JOURNAL OF THE AMERICAN CHEMICAL SOCIETY

Article

pubs.acs.org/JACS

Amine-Functionalized Lanthanide-Doped Zirconia Nanoparticles: Optical Spectroscopy, Time-Resolved Fluorescence Resonance Energy Transfer Biodetection, and Targeted Imaging

Yongsheng Liu,[†] Shanyong Zhou,[‡] Datao Tu,[†] Zhuo Chen,[‡] Mingdong Huang,[‡] Haomiao Zhu,[†,‡] En Ma,[†,‡] and Xueyuan Chen*[,†,‡]

[†]Key Laboratory of Optoelectronic Materials Chemistry and Physics and [‡]State Key Laboratory of Structural Chemistry, Fujian Institute of Research on the Structure of Matter, Chinese Academy of Sciences, Fuzhou, Fujian 350002, China

Supporting Information

ABSTRACT: Ultrasmall inorganic oxide nanoparticles doped with trivalent lanthanide ions (Ln^{3+}), a new and huge family of luminescent bioprobes, remain nearly untouched. Currently it is a challenge to synthesize biocompatible ultrasmall oxide bioprobes. Herein, we report a new inorganic oxide bioprobe based on sub-5 nm amine-functionalized tetragonal ZrO_2–Ln^{3+} nanoparticles synthesized via a facile solvothermal method and ligand exchange. By utilizing the long-lived luminescence of Ln^{3+}, we demonstrate its application as a sensitive time-resolved fluorescence resonance energy transfer (FRET) bioprobe to detect avidin with a record-low detection limit of 3.0 nM. The oxide nanoparticles also exhibit specific recognition of cancer cells overexpressed with urokinase plasminogen activator receptor (uPAR, an important marker of tumor biology and metastasis) and thus may have great potentials in targeted bioimaging.

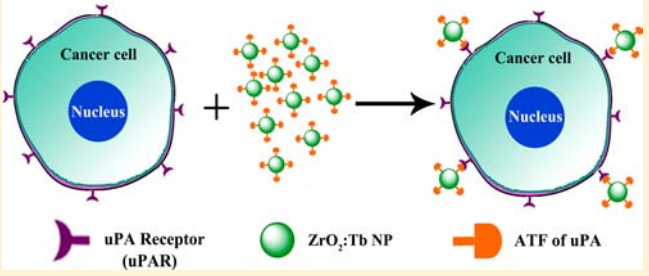

INTRODUCTION

Luminescent inorganic nanoparticles (NPs) doped with trivalent lanthanide ions (Ln^{3+}), emerging as a new class of bioprobes and as an alternative to conventional molecular probes such as lanthanide chelates and organic dyes, have attracted growing attention for their potential applications in areas as diverse as biodetection, bioimaging, and theranostics, owing to their superior features such as long photoluminescence (PL) lifetime, high chemical stability, high resistance to photobleaching, and low toxicity.[1] Hitherto, most of the previous efforts were put on the development of Ln^{3+}-doped inorganic fluoride NPs exemplified by $NaYF_4$ and $NaGdF_4$.[2] Compared to fluoride NPs, Ln^{3+}-doped inorganic oxide NPs are expected to exhibit better photostability and chemical and thermal stability because of their more rigid crystalline environment and higher lattice binding energy, which makes them highly promising as a new and huge family of luminescent bioprobes. However, it is notoriously difficult and thus remains a challenge to synthesize biocompatible bioprobes based on sub-5 nm oxide NPs. Usually oxide NPs or submicrometer crystals were prepared via coprecipitation followed by calcination or postannealing procedures, which unfortunately often result in large, aggregated, and hydrophobic NPs.[3] In particular, zirconia (ZrO_2), possessing low phonon energy (470 cm^{-1}) and high host absorption coefficient,[4] is considered as an ideal oxide host for Ln^{3+} doping to achieve intense long-lived luminescence of Ln^{3+},[5] which is the prerequisite for its bioapplications including time-resolved (TR) fluorescence resonance energy transfer (FRET) biodetection and targeted bioimaging. The TR-FRET assay, which brings together the advantage of near-zero background signal from the TR technique and the separation-free convenience of homogeneous assay from FRET, provides an excellent solution to eliminate the interference of short-lived autofluorescence from cells, tissues, and assay multiwell plate and thus offers remarkably high sensitivity as compared to the conventional FRET. Currently, TR-FRET bioprobes based on Ln^{3+}-doped inorganic NPs are very limited and restricted only to $NaYF_4$ and $KGdF_4$ NPs,[6] and there is still much room for improvement in the limit of detection (LOD) for biomolecules. As for targeted cancer cell imaging based on luminescent NPs, the key lies in their capability to recognize the specific biomarkers like receptors upregulated by cancer cells. Presently folic acid receptor and $\alpha_v\beta_3$ integrin receptor are among the most commonly used biomarkers in targeted cancer cell imaging.[7] Urokinase plasminogen activator receptor (uPAR) overexpressed in a variety of human cancer cells,[8] as another important type of prognosis marker, has never been explored in NP-based targeted imaging so far. Elevated levels of soluble uPAR in plasma or tumor tissue lysates usually indicate a poor prognosis for patient survival. Therefore, sensitive detection or monitoring of uPAR will have a significant impact on cancer diagnosis and therapy.

Received: June 21, 2012
Published: August 22, 2012

   dx.doi.org/10.1021/ja306066a | J. Am. Chem. Soc. 2012, 134, 15083–15090

In this work, sub-5 nm amine-functionalized ZrO_2–Ln^{3+} NPs were synthesized through a facile solvothermal method combined with a ligand exchange procedure. By employing the long-lived PL of Ln^{3+}, we demonstrate for the first time the use of oxide NPs (ZrO_2–Ln^{3+}) as luminescent bioprobes in a TR-FRET assay of avidin with a detection limit down to 3 nM. The use of bioconjugated ZrO_2–Ln^{3+} NPs as a feasible bioprobe for uPAR-targeted cancer cell imaging is also manifested.

RESULTS AND DISCUSSION

Monodisperse Ln^{3+}-doped ZrO_2 NPs were synthesized in the presence of capping ligands (benzyl alcohol) according to a modified solvothermal procedure reported in the literature.[5b] The as-prepared NPs are hydrophobic and readily dispersed in a variety of nonpolar organic solvents such as cyclohexane, forming a clear colloidal solution (Figure 1a). Transmission

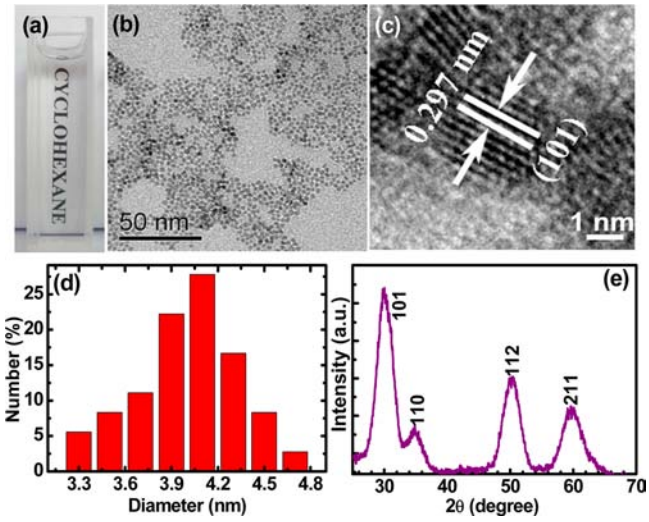

Figure 1. (a) Photograph showing the transparency of as-prepared ZrO_2–Ln^{3+} (Ln = Eu, Tb) NPs dispersed in cyclohexane solution. (b) TEM and (c) HRTEM images. (d) Histogram of size distribution. (e) XRD pattern for as-prepared ZrO_2–Ln^{3+} NPs.

electron microscopy (TEM) shows that the as-prepared NPs are roughly spherical with an average diameter of 4.1 ± 0.7 nm (Figure 1b,d). The corresponding high-resolution (HRTEM) image clearly demonstrates the high crystallinity of NPs (Figure 1c). Lattice fringes are very clear with an observed *d*-spacing of 0.297 nm, which is consistent with the lattice spacing for the (101) plane of tetragonal phase ZrO_2 (JCPDS no. 81-1545). The very small crystalline size of ZrO_2–Ln^{3+} NPs was corroborated by the broad powder X-ray diffraction (XRD) peaks that are well indexed in accordance with the standard pattern of tetragonal-phase ZrO_2 (Figure S1, Supporting Information), indicating the formation of highly crystalline ZrO_2 NPs (Figure 1e). Compositional analyses by energy-dispersive X- ray spectroscopy reveal the existence of Zr, O, and the doped Ln^{3+} ions for all ZrO_2–Ln^{3+} NPs (Figure S2, Supporting Information).

To render these hydrophobic ZrO_2–Ln^{3+} NPs biocompatible, surface modification with a hydrophilic ligand was carried out through a ligand exchange procedure.[9] 2-Aminoethyl dihydrogen phosphate (AEP) with free amine and phosphate groups was utilized to replace the native hydrophobic ligands on the surface of NPs.[10] The successful capping of AEP on the surface of ZrO_2 NPs was well established by Fourier transform infrared (FT-IR) spectrum and thermogravimetric analysis for NPs before and after ligand exchange (Figures S3 and S4, Supporting Information). As a result of surface modification, these AEP-capped NPs show much better water solubility due to the free amine groups on the NP surfaces (Figure S5, Supporting Information) and can be steadily dispersed in distilled water in the concentration range 0–0.5 mg/mL, forming a clear colloidal solution (Figure 2a,b). The ζ-potential

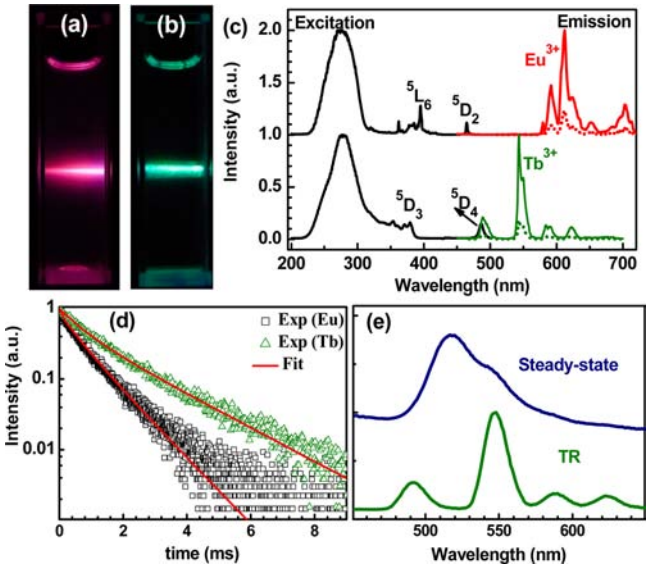

Figure 2. PL photographs for AEP-capped (a) ZrO_2–Eu^{3+} (10 mol %) and (b) ZrO_2–Tb^{3+} (10 mol %) NPs dispersed in aqueous solutions. All photographs were taken with an exposure time of 2 s upon laser excitation. (c) PL excitation (left) and PL emission (right) spectra for ZrO_2–Ln^{3+} NPs when indirectly excited at 280 nm (solid line) and directly excited at 395 nm for Eu^{3+} and at 380 nm for Tb^{3+} (dotted line). (d) PL decays of Eu^{3+} and Tb^{3+} by monitoring their emissions at 607 and 547 nm, respectively, upon UV excitation at room temperature. (e) Steady-state and time-resolved (delay time = 100 μs, gate time =1 ms) PL spectra for an aqueous solution containing 2 mM AEP-capped ZrO_2–Tb^{3+} NPs and 0.1 mM FITC.

for NP colloidal solution (pH 6.9) is +40.6 mV (Figure S6, Supporting Information), indicating the positively charged amine groups on the surface of NPs. By means of a standard Fmoc quantification protocol,[2c,11] the amount of amine group on the surfaces of NPs was estimated to be 3.58×10^{-5} mol/g, and the number of AEP conjugated to each NP was calculated to be ~9 (Figure S5, Supporting Information).

More importantly, these amine-functionalized ZrO_2–Ln^{3+} NPs were found to luminesce efficiently via host sensitization. Upon indirect excitation with a 280-nm UV laser (power density of ~15 mW/cm^2), intense red and green emissions of Eu^{3+} and Tb^{3+} ions were observed with the naked eye (Figure 2a,b). The corresponding PL excitation and emission spectra for NPs doped with Tb^{3+} or Eu^{3+} (10 mol %, the optimized doping concentration of Ln^{3+}) were measured at room temperature (RT) and are shown in Figure 2c. When the typical emissions of Eu^{3+} and Tb^{3+} at 607 nm ($^5D_0 \rightarrow {}^7F_2$) and 547 nm ($^5D_4 \rightarrow {}^7F_5$), respectively, were monitored, both the PL excitation spectra are dominated by an intense broad excitation band centered at 280 nm (Figure 2c, left), which is ascribed to the host absorption[5b] and consistent with the bandgap energy (~288 nm) determined from the UV–vis

dx.doi.org/10.1021/ja306066a | J. Am. Chem. Soc. 2012, 134, 15083–15090

absorption spectrum for pure ZrO_2 NPs (Figure S7, Supporting Information), suggesting that the Ln^{3+} emissions can be realized through an energy transfer from the host to the emitters. In sharp contrast, much weaker excitation lines originating from the $^7F_0 \rightarrow {}^5L_6$, $^5D_2$ (395 and 465 nm) transitions of Eu^{3+} and $^7F_6 \rightarrow {}^5D_3$, $^5D_4$ (380 and 487 nm) transitions of Tb^{3+} ions were detected, indicating that host sensitization is much more efficient than direct excitation of Ln^{3+}, as further confirmed by the much stronger host-sensitized PL of Eu^{3+} and Tb^{3+} than those upon direct excitation of Eu^{3+} and Tb^{3+} at 395 and 380 nm, respectively (Figure 2c and Figure S8, Supporting Information). In this energy transfer process, the excitation energy was first absorbed by the bandgap of ZrO_2 and then transferred via the ZrO_2 lattice to the emitters, where the excitation energy was released as the visible emissions of Eu^{3+} and Tb^{3+} (Figure 2c, right), respectively. These visible emissions were explicitly assigned to the typical transitions of $^5D_0 \rightarrow {}^7F_{0-4}$ and $^5D_4 \rightarrow {}^7F_{3-6}$ for Eu^{3+} and Tb^{3+}, respectively. No significant change in the PL intensities for these NPs was observed after continuous UV irradiation for 12 h (radiation density of ~0.2 W/cm^2), indicative of superior photostability of NPs (Figure S9, Supporting Information). The absolute quantum yield (QY), defined as the ratio of the number of emitted photons to the number of absorbed photons, was determined to be 32.8% and 5.2% for AEP-capped ZrO_2–Eu^{3+} and ZrO_2–Tb^{3+} NPs, respectively, which is much higher than that under direct excitation at 395 nm for Eu^{3+} (9.8%) and at 380 nm for Tb^{3+} (1.1%). The lower QY for Tb^{3+}-doped NPs is very likely due to the larger energy mismatch between the bandgap of ZrO_2 and the excited state of Tb^{3+} as well as the high-energy vibrations of capped AEP.

The PL lifetimes for these NPs were measured by monitoring the emissions of Eu^{3+} and Tb^{3+} at 607 and 547 nm, respectively. As shown in Figure 2d, the PL decays of Eu^{3+} and Tb^{3+} at RT deviate slightly from single-exponential function, which is mainly due to the superposition of decays from various sites of Ln^{3+}, for example, near-surface and lattice sites in ZrO_2 NPs. By fitting with a double-exponential function, the PL lifetimes were determined to be 0.40 (24%) and 1.02 ms (76%) for Eu^{3+}, and 0.64 (22%) and 1.82 ms (78%) for Tb^{3+} at RT, respectively (Figure 2d). Table 1 compares the optical performance of some typical Tb^{3+}-based time-resolved luminescent bioprobes including commercially available Tb-chelates.[6b,12] As shown in Table 1, ZrO_2–Tb^{3+} exhibits the largest Stokes shift with a value up to 267 nm, and its PL lifetimes of 0.64 and 1.82 ms are comparable to those of other Tb^{3+}-based time-resolved luminescent bioprobes. In comparison with short-lived autofluorescence of biological tissues and cells (usually in the nanosecond range), such long-lived PL of Ln^{3+} in ZrO_2 NPs can be readily distinguished from the undesired background fluorescence by means of TR detection. The validity of such TR detection was verified in Figure 2e, where fluorescein isothiocyanate (FITC) was intentionally selected as an artificial source of short-lived background fluorescence (~2 ns).

Table 1. Optical Properties of Typical Tb^{3+}-Based Time-Resolved Luminescent Bioprobes in Aqueous Solutions

bioprobe	lifetime (ms)	Stokes shift (nm)	ref
ZrO_2–Tb	0.64, 1.82	267	this work
Gd_2O_3–Tb	1.40	190	12a
$NaYF_4$–Ce/Tb	4.76	252	6b
LaF_3–Tb	3.20	57	12b
Tb-chelate	~1.6	225	12c
Tb-DOTA-cs124	1.54	209	12d
Tb-chelate	1.48	237	12e
Tb-BPTA	~2.0	220	12f
Tb-chelate	0.69	224	12g

The application of AEP-capped ZrO_2–Tb NPs as TR-FRET bioprobes was further explored in an avidin–biotin model system. FITC and ZrO_2–Tb NPs were selected as acceptor and donor labels, respectively, because the broad excitation peak (490 nm) of FITC overlaps well with the $^5D_4 \rightarrow {}^7F_6$ emission of Tb^{3+} at 492 nm (Figure S10, Supporting Information). Prior to the homogeneous TR-FRET assay, the covalent coupling of biotin with NPs was first carried out in *N*,*N*-dimethylformamide (DMF) solution by using *o*-benzotriazole-*N*,*N*,*N*′,*N*′-tetramethyluronium hexafluorophosphate (HBTU) and *N*,*N*-diisopropylethylamine (DIEA) as cross-linking reagents, which activated the carboxylic group of biotin and led to the formation of amide bonds between biotin and NPs (Scheme 1). Note that this bioconjugate method has never been explored in Ln^{3+} ion-doped inorganic NPs before. The FT-IR spectrum of biotinylated NPs displays a new peak at 1680 cm^{-1}, which is ascribed to the stretching vibration of amide bonds (Figure S11, Supporting Information). Accordingly, the ζ-potential for NP colloidal solution (pH 6.9) changed markedly from +40.6 to +24.2 mV after biotinylation (Figure S6, Supporting Information), as a result of the reduced amine groups and the formation of amide bonds. By using an avidin/HABA reagent,[13] the amount of biotin attached to the NPs was determined to be ~1.62 × 10^{-5} mol/g, and the number of biotin per NP was calculated to be ~3.9 (Figure S12, Supporting Information).

Scheme 1. Schematic Illustration of Biotinylation of AEP-Capped ZrO_2 NPs[a]

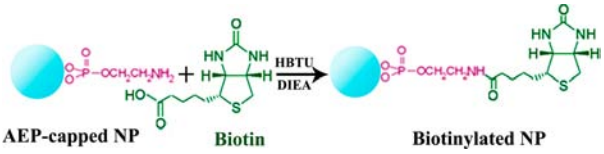

[a]The covalent coupling of biotin with NPs can be achieved in DMF solution by use of HBTU and DIEA as coupling reagents.

The principle for homogeneous TR-FRET assay is schematically illustrated in Figure 3a. Briefly, after addition of 100 μL of biotinylated NPs (50 μg/mL) to the wells of a 96-well microplate, different amounts of FITC-labeled avidin were added to each well and then the plate was incubated at 37 °C for 30 min, during which the biotinylated NPs were conjugated with avidin via a sensitive and specific interaction between avidin and biotin. The microplate was subjected to TR-FRET measurements on a microplate reader (BioTeK). The concentration of avidin can be quantified by measuring the integrated PL intensity ratio of FITC and Tb^{3+} denoted by $FITC_{520}/Tb_{492}$, a figure of merit derived from the deconvolution of the TR-FRET spectrum (Figure S13, Supporting Information). As shown in Figure 3b, the TR-FRET signal represented by $FITC_{520}$ was gradually enhanced at the expense of Tb_{492} with increasing amount of FITC-labeled avidin, thus verifying the specific binding and FRET occurrence. For comparison, nonbinding control experiments were performed by employing the AEP-capped NPs instead of the biotinylated

dx.doi.org/10.1021/ja306066a | J. Am. Chem. Soc. 2012, 134, 15083–15090

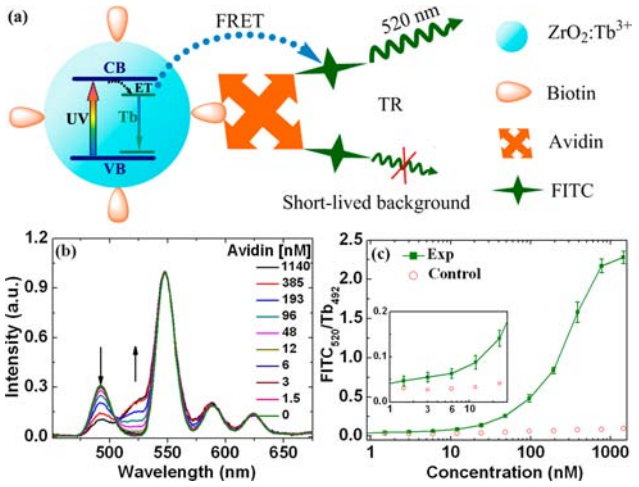

Figure 3. (a) Schematic illustration showing the principle of TR-FRET detection of avidin by employing biotinylated ZrO_2–Tb NPs as donor and FITC-labeled avidin as acceptor. VB and CB denote as the valence and conduction bands, respectively. (b) TR-FRET spectra of the bioassays as a function of avidin concentration. All the spectra were normalized to unity at the maximum emission peak at 547 nm, and each data point represents average of triplicate measurements. (c) Calibration curve of TR-FRET detection for the integrated PL intensity ratio $FITC_{520}/Tb_{492}$ versus the concentration of avidin.

NPs as bioprobes under otherwise identical conditions. The calibration curve (Figure 3c) demonstrates that the TR-FRET signal of $FITC_{520}/Tb_{492}$ gradually increases with avidin concentration ranging from 0.75 to 1140 nM and tends to saturate at higher concentration than 1000 nM. Nonbiotinylated NPs and FITC were far apart in the solution and thus no FRET occurred in the control experiments (Figure S14, Supporting Information). As a result, the TR-FRET signals were hardly observed in the control experiments. The limit of detection (LOD), defined as the concentration that corresponds to 3 times the standard deviation above the signal measured in the control experiment, is 3.0 nM, which is presently the lowest relative to fluoride-based TR-FRET bioprobes previously reported (Table 2).[6] The improvement

Table 2. Limit of Detection for Biomolecules Based on Some Typical FRET Bioprobes

bioprobe	size (nm)	assay type	analyte	LOD (nM)	ref
ZrO_2–Tb	<5	TR-FRET	avidin	3	this work
$NaYF_4$–Ce,Tb	20–40	TR-FRET	avidin	4.8	6b
$KGdF_4$–Tb	20–30	TR-FRET	avidin	5.5	6a
$NaYF_4$–Yb,Er	~50	UC-FRET	avidin	~0.5	14a
CdSe/ZnS QDs	10–15	FRET	avidin	10	14b
$NaYF_4$–Yb,Er	20–90	UC-FRET	IgG	~6	14c
$NaYF_4$–Yb,Er	14	UC-FRET	DNA	~10	1e
LaF_3–Ce,Tb	15–20	FRET	glucose	~0.5	14d

of LOD may be attributed to the much smaller size (~5 nm) of ZrO_2 NPs that is more advantageous in distance-dependent FRET biodetection than the larger fluoride NPs. Table 2 also compares the LOD for various biomolecules achieved by using some other FRET bioprobes. The LOD of avidin achieved by using sub-5 nm ZrO_2–Tb^{3+} NPs is comparable to those based on the upconversion (UC) FRET or steady-state competitive FRET assay that utilized $NaYF_4$–Yb/Er NPs (or quantum dots, QDs) as bioprobes to detect biomolecules such as avidin, DNA, IgG, and glucose with LOD of 0.5–10 nM.[1e,14] Note that the LOD for other types of assays such as competitive and noncompetitive (or sandwich-type) heterogeneous assay could be as low as several to tens of picomoles per liter,[15] which is much lower than those for homogeneous assays like TR-FRET and UC-FRET (Table 2). However, one should keep in mind that the heterogeneous assay is labor-intensive and time-consuming due to the tedious separation and washing steps before signal measurement, which is inconvenient for fast biodetection in some practical applications.[15a]

Another important application for these sub-5 nm ZrO_2 NPs is targeted cancer cell imaging. To achieve successful cellular imaging targeted at uPAR, the amino-terminal fragment (ATF) of urokinase plasminogen activator, which has high binding affinity ($K_d \approx 0.28$ nM)[16] and specific interaction with uPAR highly expressed on the membrane of many types of cancer cells such as human lung cancer cell (H1299), was covalently linked to the surface of amine-functionalized ZrO_2–Tb NPs by using the same biological coupling reagents for NP biotinylation. The amount of ATF linked to the surface of NPs was roughly estimated to be 2.19×10^{-6} mol/g (~0.53 ATF molecule/NP) by use of the commercial bicinchoninic acid (BCA) protein assay kit and bovine serum albumin (BSA) as a reference (Figure S15, Supporting Information). The specific recognition capability of ATF-coupled NPs was then examined by means of confocal laser scanning microscopy (CLSM). Due to the high binding affinity between ATF and uPAR, the ATF-coupled NPs can be specifically targeted to the membrane of H1299 cells after incubation in phosphate-buffered saline (PBS) at 37 °C for 2 h (Scheme 2). As a result,

Scheme 2. Schematic Illustration Showing the Specific Recognition of ZrO_2:Tb-ATF NPs to H1299 Cancer Cells with uPAR High Expression

intense Tb^{3+} green signal (green channel) was observed on the surface of H1299 cells upon 488-nm laser excitation (Figure 4a). Meanwhile, we also measured the bright-field images as well as blue-channel images showing the location of the 4′,6-diamidino-2-phenylindole (DAPI) stained cell nuclei of H1299 cells. The overlay of the green-channel, blue-channel, and bright-field images (Figure 4a) shows unambiguously that the intense Tb^{3+} signals originated from ATF-coupled NPs bound to the membrane of H1299 cells. For comparison, the control experiment of CLSM imaging was carried out on human embryo lung fibroblasts (HELF) cells with uPAR low-expressed under identical imaging conditions. As shown in Figure 4b, the Tb^{3+} green signals were hardly observed on the surface of HELF cells due to the lack of specific recognition between the ATF-coupled NPs and HELF cells. These results clearly demonstrate that ATF-coupled NPs can be used as a feasible

dx.doi.org/10.1021/ja306066a | J. Am. Chem. Soc. 2012, 134, 15083–15090

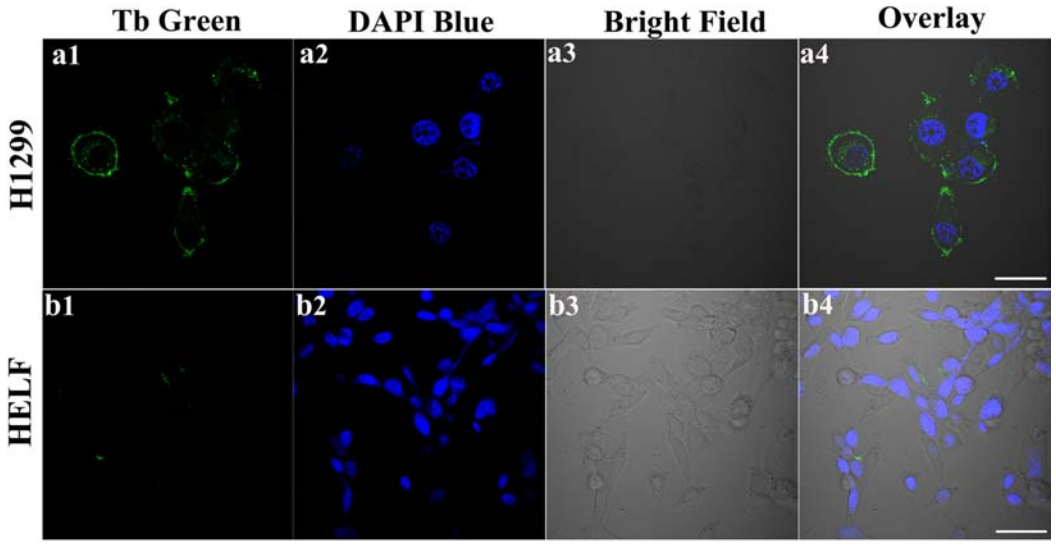

Figure 4. CLSM images of (a) H1299 and (b) HELF cells after incubation with ZrO_2−Tb-ATF NPs (1 mg/mL) for 2 h at 37 °C. Tb green emissions are shown in panel 1 (λ_{em} = 500−560 nm, λ_{ex} = 488 nm). DAPI blue images (λ_{em} = 450−490 nm, λ_{ex} = 405 nm) that indicate the nuclear regions are shown in panel 2. Panel 3 is the bright-field image that outlines the position of cells, and panel 4 is the overlay image of panels 1, 2, and 3 (scale bar = 30 μm).

bioprobe for targeted imaging of cancer cells with uPAR overexpressed, which had not been revealed before.

One key issue for practical bioapplications is the dark cytotoxicity and phototoxicity of NPs when applied in targeted bioimaging. The dark cytotoxicity and phototoxicity for the ATF-coupled ZrO_2−Tb NPs were determined on the HELF cells by using a cell counting kit (CCK-8) assay.[17] As shown in Figure 5, the cell viability was determined to be larger than 91%

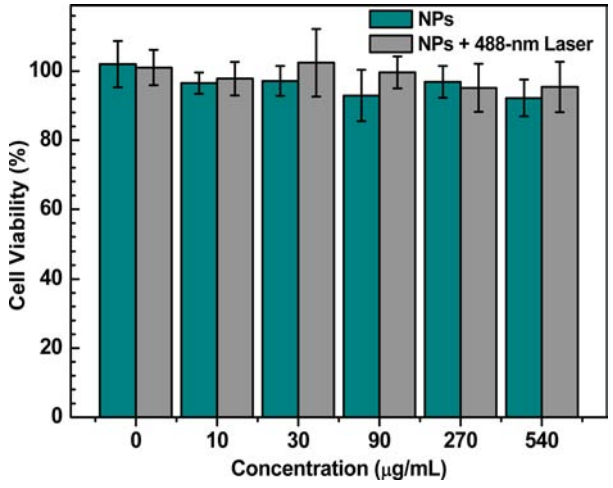

Figure 5. In vitro dark cytotoxicity and phototoxicity of ATF-coupled ZrO_2−Tb NPs against HELF cells after 4 h incubation.

even at a concentration as high as 540 μg/mL ATF-coupled NPs both in the dark and upon a 488-nm laser irradiation for 2 min. Such low dark cytotoxicity and phototoxicity infer that the oxide NP probe is biocompatible and nearly nontoxic to live cells.

CONCLUSIONS

In summary, we have developed a new inorganic oxide biolabel based on amine-functionalized tetragonal ZrO_2−Ln^{3+} NPs with small size (ca. 5.0 nm) via a modified solvothermal method and ligand exchange procedure. A new bioconjugate method was also proposed to achieve quantitative bioconjugation between amine-functionalized ZrO_2−Ln^{3+} NPs and various biomolecules including biotin and ATF. Intense visible emissions from Ln^{3+} ions can be achieved in ZrO_2 NPs through host sensitization. By utilizing the distinct optical properties and long-lived luminescence of Ln^{3+}, we have demonstrated for the first time the application of biotinylated ZrO_2 NPs as a sensitive TR-FRET bioprobe to detect avidin with a record-low detection limit of 3.0 nM. Furthermore, ZrO_2−Tb NPs bioconjugated with ATF of uPA exhibited specific recognition capability for cancer cells overexpressed with uPAR, a marker of tumor biology and metastasis, and thus have great potential as an imaging probe for targeting various cancer cells. These findings may open up new avenues for the exploration of Ln^{3+}-doped oxide-based NPs in versatile bioapplications like TR biodetection and bioimaging. The proposed approaches could be further extended to other new luminescent bioprobes based on Ln^{3+}-doped inorganic oxide NPs that remain nearly untouched.

EXPERIMENTAL DETAILS

Chemicals and Materials. Zirconium(IV) propoxide propanol, benzyl alcohol, acetone, *N*,*N*-dimethylformamide (DMF), and ethanol were purchased from Sinopharm Chemical Reagent Co., China. Fluorescein isothiocyanate (FITC), *o*-benzotriazole-*N*,*N*,*N*′,*N*′-tetramethyluronium hexafluorophosphate (HBTU), *N*,*N*-diisopropylethylamine (DIEA), 4′-hydroxyazobenzene-2-carboxylic acid (HABA), nitrosyl tetrafluoroborate ($NOBF_4$), 4′,6-diamidino-2-phenylindole (DAPI), avidin, and biotin were purchased from Sigma−Aldrich (China). 2-Aminoethyl dihydrogen phosphate (AEP) was purchased from TCI (Shanghai) Development Co., Ltd. Amino-terminal fragment (ATF) of urokinase plasminogen activator (uPA) (residues 1−143 of uPA) was expressed in yeast cell (*Pichia pastoris*) to ensure proper protein folding and purified following the procedure previously described.[18] The opaque 96-well microtitration microplate (Costar 3922) was purchased from Corning Inc. All chemical reagents were of analytical grade and were used as received without further purification.

Synthesis of ZrO_2−Ln^{3+} NPs. Monodisperse ZrO_2−Ln^{3+} NPs (Ln = Eu, Tb) were synthesized according to a modified solvothermal procedure reported in the literature.[5b] Briefly, 0.6 mmol of

$Eu(CH_3COO)_3{\cdot}6H_2O$ or 0.6 mmol of $Tb(CH_3COO)_3{\cdot}6H_2O$ was dissolved and well stirred in a mixed solution containing 20 mL of benzyl alcohol and 1.6 mL of zirconium(IV) propoxide propanol (70 wt %) to form a transparent solution. Thereafter, the transparent solution was transferred into a 50-mL Teflon-lined autoclave and heated at 230 °C for 72 h. After the solution cooled to RT naturally, the resulting ZrO_2–Ln^{3+} NPs were precipitated by addition of ethanol, collected by centrifugation at 12 000 rpm for 3 min, washed with ethanol several times, and finally redispersed in cyclohexane. The overall yield of the final product was estimated to be ~81% based on the starting materials.

Synthesis of Amine-Functionalized ZrO_2–Ln^{3+} NPs. The surface amine functionalization of the as-prepared ZrO_2–Ln^{3+} NPs was carried out by using a modified ligand exchange strategy.[9] In a typical process, 20 mL of cyclohexane solution containing 20 mg of NPs was mixed with 15 mL of dichloromethane solution of $NOBF_4$ (0.005 M) at RT and vigorously stirred for 10 min to yield white precipitates, which were collected by centrifugation at 12 000 rpm for 4 min, and redispersed in 20 mL of DMF to form a transparent solution. Subsequently, 0.1 mmol AEP was added to the above transparent solution. After the solution was stirred for 60 min at RT, amine-functionalized ZrO_2–Ln^{3+} NPs were obtained by adding 20 mL of acetone, centrifuging, and washing with DMF and water several times to remove the excess AEP. The final products were dispersed in water and stored at 4 °C for the following use.

Synthesis of Biotinylated ZrO_2–Ln^{3+} NPs. Different from the most common EDC/NHS protocol performed in biological buffers within the pH range 4.5–7.5,[6a,14a] the successful bioconjugation of amine-functionalized ZrO_2–Ln^{3+} NPs with biotin was easily achieved in DMF solution by utilizing HBTU and DIEA as coupling reagents. Note that the following protocol had never been explored in Ln^{3+}-doped inorganic NPs before this work. In a typical procedure, 20 mg of biotin and 37 mg of HBTU were first added into a solution of 0.9 mL of DMF and 0.1 mL of DIEA. The mixture was incubated at RT for 6 h to activate the carboxylic group of biotin. Thereafter, 20 mg of amine-functionalized ZrO_2–Ln^{3+} NPs was dissolved in the above solution and sonicated for 5 min. The coupling reaction between carboxylic group of biotin and amine group of NPs was allowed to proceed at 4 °C overnight with continuous shaking. Biotinylated ZrO_2–Ln^{3+} NPs were obtained by centrifugation and washing with DMF and distilled water several times to remove the excess biotin, HBTU, and DIEA. Finally, biotinylated NPs were dispersed in water and stored at 4 °C for TR-FRET biodetection.

Quantitative Analysis of Amine Groups on the Surface of AEP-Capped ZrO_2–Ln^{3+} NPs. The amount of amine groups bound to the surface of ZrO_2–Ln^{3+} NPs was estimated by using Fmoc protection and a standard Fmoc quantification protocol.[2c,11] Briefly, 25 mg of FmocCl was added to 3 mL of anhydrous DMF solution containing 20 mg of AEP-capped ZrO_2–Ln^{3+} NPs. The above mixture was stirred overnight under N_2 at RT and then centrifuged at 12 000 rpm for 4 min to separate AEP-capped ZrO_2 NPs with complete Fmoc protection of their amine groups. The resulting Fmoc-protected products were then thoroughly washed several times with methanol and dried in vacuum overnight. The Fmoc-protected ZrO_2 NPs were precisely weighed in an Eppendorf tube and resuspended in 2.5 mL of DMF. Subsequently, 1 mL of piperidine was added to the above solution for Fmoc cleavage. The cleavage mixture containing the NPs was sonicated for over 20 min. After centrifugation at 13 200 rpm for 10 min, the amine groups bound to the surface of ZrO_2 NPs can be quantified by means of the standard Fmoc quantification protocol based on the measurement of UV absorbance of the supernatant Fmoc solution at 300 nm, at which wavelength the extinction coefficient of Fmoc is 7800 $mol^{-1}{\cdot}dm^3{\cdot}cm^{-1}$.

Quantitative Analysis of Biotin in Biotinylated ZrO_2–Ln^{3+} NPs. The amount of biotin conjugated to the surface of AEP-capped ZrO_2 NPs can be determined by using the avidin/4′-hydroxyazobenzene-2-carboxylic acid (HABA) reagent.[13] The HABA dye can be bound to avidin to produce a yellow-orange colored complex that absorbs at 500 nm. When biotinylated sample is mixed with the HABA–avidin complex solution, biotin will displace the HABA dye and cause the absorbance to decrease. In our experiment, the HABA solution was prepared by adding HABA (24.2 mg) into deionized water (10 mL), followed by the addition of 0.2 mL of NaOH (1 M). The undissolved HABA particulates were removed by filtration. The avidin–HABA complex solution was prepared by dissolving avidin (5 mg) in 50 mL of PBS, followed by the addition of 0.3 mL of HABA solution. One milligram of biotinylated ZrO_2–Ln^{3+} NPs for avidin/HABA assay was dissolved in 0.033 mL of PBS (50 mM, pH 7.1) and mixed with 0.3 mL of avidin–HABA solution. The amount of biotin in biotinylated ZrO_2–Ln^{3+} NPs can be determined by a calibration curve generated by adding a known amount of biotin in the avidin/HABA solution sequentially, followed by recording the absorbance at 500 nm.

Bioconjugation of Amine-Functionalized ZrO_2–Ln^{3+} NPs with ATF. The bioconjugation of amine-functionalized ZrO_2–Ln^{3+} NPs with ATF is similar to the biotinlyation of ZrO_2 NPs. Briefly, 10 mg of ATF and 10 mg of HBTU were first dissolved in a solution of 0.9 mL of DMF and 0.1 mL of DIEA. After the activation of ATF at RT for 30 min, 20 mg of amine-functionalized ZrO_2–Ln^{3+} NPs was added to the above solution and sonicated for 5 min. The mixture solution was then allowed to shake gently overnight at 4 °C. Finally, the ATF-coupled ZrO_2 NPs were obtained by centrifugation and washing with DMF and distilled water several times. The resulting ATF-coupled ZrO_2 NPs were dispersed in water and stored at 4 °C for targeted cancer cell imaging.

Quantitative Analysis of ATF on the Surface of ZrO_2–Ln^{3+} NPs. The amount of ATF coupled to ZrO_2 NPs can be approximately quantified on the basis of a standard BCA protein assay protocol.[19] The micro BCA protein assay reagent kit was ordered from Sigma–Aldrich. A standard curve was prepared as described in the protocol. The ATF content on the surface of ATF-coupled ZrO_2–Tb NPs was determined from the standard curve with BSA as a reference.

Synthesis of FITC-Labeled Avidin. The avidin protein was labeled with FITC via a well-established protocol previously summarized by Hermanson.[20] In brief, 10 mg of avidin was dissolved in 5 mL of sodium carbonate buffer (0.1 M, pH 9.5). Meanwhile, 2 mg of FITC was dissolved in 1 mL of DMF. Then the two solutions were mixed and reacted overnight at 4 °C in the dark. The excess FITC was removed via extensive dialysis for 48 h using a membrane of molecular weight cutoff of 10 000. FITC quantification was performed by detection with UV absorption of the solution at λ = 494 nm. The extinction coefficient at this wavelength for FITC is 70 000 $M^{-1}{\cdot}cm^{-1}$. The number of FITC per avidin molecule was approximately determined to be 2.3.

Homogeneous TR-FRET Detection of Avidin Based on Biotinylated ZrO_2–Tb^{3+} NPs. Biotinylated ZrO_2–Tb^{3+} solution (100 μL, 50 μg/mL) was added to the wells of a 96-well microplate, and then 100 μL of FITC-labeled avidin with different concentrations was added. After incubation for 30 min at RT, the plate was subjected to TR-FRET detection on a multimodal microplate reader (Synergy 4, BioTeK) at RT. The excitation wavelength was 280 nm, and the delay time and gate time were set to be 100 μs and 10 ms, respectively. For comparison, control experiments were performed by employing nonbiotinylated NP counterparts as bioprobes under otherwise identical conditions. Every measurement was repeated three times to give the average values.

Cell Culture and Confocal Laser Scanning Microscopy in Vitro. H1299 and HELF cell lines were purchased from Shanghai Institute of Cell Biology, Chinese Academy of Sciences, and were routinely maintained in RPMI-1640 mediym (Gibco BRL), supplemented with 10% (v/v) heat-inactivated fetal calf serum, penicillin (100 units·mL^{-1}), and streptomycin (100 units·mL^{-1}) at 37 °C under humidified air containing 5% CO_2. Cells were seeded into culture plates and allowed to adhere for 24 h. After being washed with PBS, the cells were incubated in PBS buffer containing 0.5 mg/mL ATF-coupled ZrO_2–Tb^{3+} NPs at 37 °C for 2 h under 5% CO_2 and then washed with PBS sufficiently to remove excess NPs. The cells were subsequently incubated with DAPI at RT for 5 min and washed with PBS. The cell imaging was performed on a confocal laser scanning microscope equipped with an Olympus FV1000 scanning unit. Cells were excited by a 488-nm laser with maximum output

power of ~0.7 mW, and the luminescence signals were detected in the green channel (500−560 nm) and blue channel (450−490 nm).

Dark Cytotoxicity and Phototoxicity of ATF-Coupled ZrO_2−Tb NPs. The dark cytotoxicity of ATF-coupled ZrO_2−Tb NPs was tested by using the CCK-8 assays on the HELF cells. In brief, HELF cells were seeded into a 96-well cell culture plate at 2×10^4/well and cultured at 37 °C under humidified air containing 5% CO_2 for 24 h before the addition of different concentrations of ATF-coupled ZrO_2−Tb NPs (0, 10, 30, 90, 270, and 540 μg/mL, diluted in RPMI 1640) to the wells. The HELF cells were then incubated at 37 °C under 5% CO_2 for 4 h. CCK-8 was subsequently applied to the cells, followed by incubation at 37 °C under 5% CO_2 for 4 h. The OD_{450} value of each well was measured on a multimodal microplate reader (Synergy 4, BioTek). The following formula was applied to calculate the percent inhibition rate of cell growth: cell viability (%) = (mean of absorbance value of treatment group/mean of absorbance value of control) × 100. Almost the same protocol was utilized to determine the phototoxicity of ATF-coupled ZrO_2−Tb NPs, except that the HELF cells were irradiated by using a 488-nm laser (power density of ~20 mW/cm^2) for 2 min after incubation of the ATF-coupled ZrO_2−Tb NPs with HELF cells for 4 h.

Characterization. XRD patterns of the samples were collected on an X-ray diffractometer (MiniFlex2, Rigaku) with Cu Kα1 radiation (λ = 0.154 187 nm). Both the low- and high-resolution TEM measurements were performed on a JEOL-2010 TEM equipped with the energy-dispersive X-ray spectrum. Thermogravimetric analyses were conducted on a Netzsch STA449C thermal analysis system under N_2 atmosphere flow at a rate of 10 °C/min. FT-IR spectra were recorded in KBr discs on a Magna 750 FT-IR spectrometer. The ζ-potential of AEP-capped or biotinylated ZrO_2 NPs dispersed in distilled water (pH 6.9) was determined by means of dynamic light scattering (DLS) measurement (Nano ZS ZEN3600, Malvern). PL emission and excitation spectra and PL lifetimes were recorded on a spectrometer equipped with both continuous (450 W) xenon and pulsed flash lamps (FLS920, Edinburgh Instrument). The absolute quantum yield of ZrO_2−Ln^{3+} NPs was measured at RT by employing a barium sulfate-coated integrating sphere (Edinburgh) as the sample chamber that was mounted on the FLS920 spectrometer, with the entry and output port of the sphere located in 90° geometry from each other in the plane of the spectrometer. All the spectral data collected were corrected for the spectral response of both the spectrometer and the integrating sphere. PL photographs of the NP solutions were taken with Nikon digital single lens reflex D100 upon excitation by the third-harmonic generation (THG) of a mode-locked picosecond Ti:sapphire laser (~1 mW@280 nm, Tsunami, Spectra-Physics). The TR-FRET spectra were measured on a multimodal microplate reader (Synergy 4, BioTek). Confocal imaging of cells was performed with a modified Olympus FV1000 laser scanning confocal microscope (60× oil-immersion objective len).

■ ASSOCIATED CONTENT

Supporting Information

Fifteen figures as described in the text. This material is available free of charge via the Internet at http://pubs.acs.org.

■ AUTHOR INFORMATION

Corresponding Author

xchen@fjirsm.ac.cn

Notes

The authors declare no competing financial interest.

■ ACKNOWLEDGMENTS

This work is supported by the NSFC (Nos. 10974200, 11004191, 51102234, and 11104266), the 863 program of MOST (No. 2011AA03A407), and the NSF of Fujian Province for Young Scientists (Nos. 2010J05126 and 2011J05145). We thank Prof. Fuyou Li and Ms. Qian Liu for their kindly help in the targeted cancer cell imaging.

■ REFERENCES

(1) (a) Wang, F.; Han, Y.; Lim, C. S.; Lu, Y. H.; Wang, J.; Xu, J.; Chen, H. Y.; Zhang, C.; Hong, M. H.; Liu, X. G. *Nature* **2010**, *463*, 1061. (b) Vetrone, F.; Naccache, R.; Mahalingam, V.; Morgan, C. G.; Capobianco, J. A. *Adv. Funct. Mater.* **2009**, *19*, 2924. (c) Kumar, R.; Nyk, M.; Ohulchanskyy, T. Y.; Flask, C. A.; Prasad, P. N. *Adv. Funct. Mater.* **2009**, *19*, 853. (d) Li, Z. Q.; Zhang, Y.; Jiang, S. *Adv. Mater.* **2008**, *20*, 4765. (e) Chen, Z. G.; Chen, H. L.; Hu, H.; Yu, M. X.; Li, F. Y.; Zhang, Q.; Zhou, Z. G.; Yi, T.; Huang, C. H. *J. Am. Chem. Soc.* **2008**, *130*, 3023. (f) Zhou, J.; Sun, Y.; Du, X. X.; Xiong, L. Q.; Hu, H.; Li, F. Y. *Biomaterials* **2010**, *31*, 3287. (g) Yi, G. S.; Chow, G. M. *Chem. Mater.* **2007**, *19*, 341. (h) Haase, M.; Schafer, H. *Angew. Chem., Int. Ed.* **2011**, *50*, 5808. (i) Wang, J.; Tanner, P. A. *J. Am. Chem. Soc.* **2009**, *132*, 947. (j) Shen, J.; Sun, L. D.; Zhu, J. D.; Wei, L. H.; Sun, H. F.; Yan, C. H. *Adv. Funct. Mater.* **2010**, *20*, 3708. (k) Wang, G. F.; Peng, Q.; Li, Y. D. *Acc. Chem. Res.* **2011**, *44*, 322. (l) Zhang, F.; Braun, G. B.; Pallaoro, A.; Zhang, Y.; Shi, Y.; Cui, D.; Moskovits, M.; Zhao, D.; Stucky, G. D. *Nano Lett.* **2011**, *12*, 61. (m) Mader, H. S.; Kele, P.; Saleh, S. M.; Wolfbeis, O. S. *Curr. Opin. Chem. Biol.* **2010**, *14*, 582. (n) Stouwdam, J. W.; van Veggel, F. C. J. M. *Nano Lett.* **2002**, *2*, 733. (o) Mahalingam, V.; Vetrone, F.; Naccache, R.; Speghini, A.; Capobianco, J. A. *Adv. Mater.* **2009**, *21*, 4025. (p) Heer, S.; Lehmann, O.; Haase, M.; Güdel, H. U. *Angew. Chem., Int. Ed.* **2003**, *42*, 3179. (q) Liu, Q.; Sun, Y.; Yang, T. S.; Feng, W.; Li, C. G.; Li, F. Y. *J. Am. Chem. Soc.* **2011**, *133*, 17122. (r) Zhou, J.; Zhu, X.; Chen, M.; Sun, Y.; Li, F. *Biomaterials* **2012**, *33*, 6201.

(2) (a) Zhou, J.; Liu, Z.; Li, F. Y. *Chem. Soc. Rev.* **2012**, *41*, 1323. (b) Wang, C.; Tao, H. Q.; Cheng, L.; Liu, Z. *Biomaterials* **2011**, *32*, 6145. (c) Cao, T. Y.; Yang, Y.; Gao, Y. A.; Zhou, J.; Li, Z. Q.; Li, F. Y. *Biomaterials* **2011**, *32*, 2959. (d) Liu, Q.; Peng, J. J.; Sun, L. N.; Li, F. Y. *ACS Nano* **2011**, *5*, 8040. (e) Jalil, R. A.; Zhang, Y. *Biomaterials* **2008**, *29*, 4122. (f) Liu, Y. S.; Tu, D. T.; Zhu, H. M.; Li, R. F.; Luo, W. Q.; Chen, X. Y. *Adv. Mater.* **2010**, *22*, 3266. (g) Hou, Z. Y.; Li, C. X.; Ma, P. A.; Li, G. G.; Cheng, Z. Y.; Peng, C.; Yang, D. M.; Yang, P. P.; Lin, J. *Adv. Funct. Mater.* **2011**, *21*, 2356. (h) Wang, F.; Deng, R. R.; Wang, J.; Wang, Q. X.; Han, Y.; Zhu, H. M.; Chen, X. Y.; Liu, X. G. *Nat. Mater.* **2011**, *10*, 968. (i) Zhang, F.; Shi, Q. H.; Zhang, Y. C.; Shi, Y. F.; Ding, K. L.; Zhao, D. Y.; Stucky, G. D. *Adv. Mater.* **2011**, *23*, 3775. (j) Achatz, D. E.; Meier, R. J.; Fischer, L. H.; Wolfbeis, O. S. *Angew. Chem., Int. Ed.* **2011**, *50*, 260. (k) Gai, S. L.; Yang, P. P.; Li, C. X.; Wang, W. X.; Dai, Y. L.; Niu, N.; Lin, J. *Adv. Funct. Mater.* **2010**, *20*, 1166. (l) Boyer, J. C.; Manseau, M. P.; Murray, J. I.; van Veggel, F. C. J. M. *Langmuir* **2010**, *26*, 1157. (m) Chen, G.; Ohulchanskyy, T. Y.; Liu, S.; Law, W.-C.; Wu, F.; Swihart, M. T.; Ågren, H.; Prasad, P. N. *ACS Nano* **2012**, *6*, 2969. (n) Wang, F.; Sun, L.; Gu, J.; Wang, Y.; Feng, W.; Yang, Y.; Wang, J.; Yan, C. *Angew. Chem., Int. Ed.* **2012**, DOI: 10.1002/anie.201203069. (o) Park, Y. I.; Kim, J. H.; Lee, K. T.; Jeon, K.-S.; Na, H. B.; Yu, J. H.; Kim, H. M.; Lee, N.; Choi, S. H.; Baik, S.; Kim, H.; Park, S. P.; Park, B. J.; Kim, Y. W.; Lee, S. H.; Yoon, S. Y.; Song, I. C.; Moon, W. K.; Suh, Y. D.; Hyeon, T. *Adv. Mater.* **2009**, *21*, 4467.

(3) (a) Jadhav, A. P.; Pawar, A.; Kim, C. W.; Cha, H. G.; Pal, U.; Kang, Y. S. *J. Phys. Chem. C* **2009**, *113*, 16652. (b) Liu, H. Q.; Wang, L. L.; Chen, S. G.; Zhou, B. S.; Peng, Z. W. *Appl. Surf. Sci.* **2007**, *253*, 3872. (c) Ye, X. C.; Collins, J. E.; Kang, Y. J.; Chen, J.; Chen, D. T. N.; Yodh, A. G.; Murray, C. B. *Proc. Natl. Acad. Sci. U.S.A.* **2010**, *107*, 22430.

(4) (a) Sato, K.; Abe, H.; Ohara, S. *J. Am. Chem. Soc.* **2010**, *132*, 2538. (b) Joo, J.; Yu, T.; Kim, Y. W.; Park, H. M.; Wu, F. X.; Zhang, J. Z.; Hyeon, T. *J. Am. Chem. Soc.* **2003**, *125*, 6553.

(5) (a) Jiang, C. L.; Wang, F.; Wu, N. Q.; Liu, X. G. *Adv. Mater.* **2008**, *20*, 4826. (b) Ninjbadgar, T.; Garnweitner, G.; Börger, A.; Goldenberg, L. M.; Sakhno, O. V.; Stumpe, J. *Adv. Funct. Mater.* **2009**, *19*, 1819. (c) Qu, X.; Song, H.; Pan, G.; Bai, X.; Dong, B.; Zhao, H.; Dai, Q.; Zhang, H.; Qin, R.; Lu, S. *J. Phys. Chem. C* **2009**, *113*, 5906. (d) Julian, B.; Corberan, R.; Cordoncillo, E.; Escribano, P.; Viana, B.;

Sanchez, C. *Nanotechnology* **2005**, *16*, 2707. (e) Lue, Q.; Guo, F.; Sun, L.; Li, A.; Zhao, L. *J. Phys. Chem. C* **2008**, *112*, 2836. (f) Romero, V. H.; De la Rosa, E.; Lopez-Luke, T.; Salas, P.; Angeles-Chavez, C. *J. Phys. D: Appl. Phys.* **2010**, *43*, No. 465105.
(6) (a) Ju, Q.; Tu, D. T.; Liu, Y. S.; Li, R. F.; Zhu, H. M.; Chen, J. C.; Chen, Z.; Huang, M. D.; Chen, X. Y. *J. Am. Chem. Soc.* **2012**, *134*, 1323. (b) Tu, D. T.; Liu, L. Q.; Ju, Q.; Liu, Y. S.; Zhu, H. M.; Li, R. F.; Chen, X. Y. *Angew. Chem., Int. Ed.* **2011**, *50*, 6306.
(7) (a) Hu, H.; Xiong, L. Q.; Zhou, J.; Li, F. Y.; Cao, T. Y.; Huang, C. H. *Chem.—Eur. J.* **2009**, *15*, 3577. (b) Xiong, L. Q.; Chen, Z. G.; Tian, Q. W.; Cao, T. Y.; Xu, C. J.; Li, F. Y. *Anal. Chem.* **2009**, *81*, 8687.
(8) (a) Huai, Q.; Mazar, A. P.; Kuo, A.; Parry, G. C.; Shaw, D. E.; Callahan, J.; Li, Y. D.; Yuan, C.; Bian, C. B.; Chen, L. Q.; Furie, B.; Furie, B. C.; Cines, D. B.; Huang, M. D. *Science* **2006**, *311*, 656. (b) Blasi, F.; Carmeliet, P. *Nat. Rev. Mol. Cell Biol.* **2002**, *3*, 932.
(9) Dong, A. G.; Ye, X. C.; Chen, J.; Kang, Y. J.; Gordon, T.; Kikkawa, J. M.; Murray, C. B. *J. Am. Chem. Soc.* **2011**, *133*, 998.
(10) Dong, C. H.; Raudsepp, M.; van Veggel, F. C. J. M. *J. Phys. Chem. C* **2009**, *113*, 472.
(11) Yoon, T. J.; Yu, K. N.; Kim, E.; Kim, J. S.; Kim, B. G.; Yun, S. H.; Sohn, B. H.; Cho, M. H.; Lee, J. K.; Park, S. B. *Small* **2006**, *2*, 209.
(12) (a) Louis, C.; Bazzi, R.; Marquette, C. A.; Bridot, J. L.; Roux, S.; Ledoux, G.; Mercier, B.; Blum, L.; Perriat, P.; Tillement, O. *Chem. Mater.* **2005**, *17*, 1673. (b) Sivakumar, S.; Diamente, P. R.; van Veggel, F. C. *Chem.—Eur. J.* **2006**, *12*, 5878. (c) Geißler, D.; Charbonnière, L. J.; Ziessel, R. F.; Butlin, N. G.; Löhmannsröben, H.-G.; Hildebrandt, N. *Angew. Chem., Int. Ed.* **2010**, *49*, 1396. (d) Li, M.; Selvin, P. R. *J. Am. Chem. Soc.* **1995**, *117*, 8132. (e) Charbonniere, L. J.; Hildebrandt, N.; Ziessel, R. F.; Loehmannsroeben, H. G. *J. Am. Chem. Soc.* **2006**, *128*, 12800. (f) Sueda, S.; Yuan, J. L.; Matsumoto, K. *Bioconjugate Chem.* **2002**, *13*, 200. (g) Huhtinen, P.; Kivela, M.; Kuronen, O.; Hagren, V.; Takalo, H.; Tenhu, H.; Lovgren, T.; Harma, H. *Anal. Chem.* **2005**, *77*, 2643.
(13) Wang, X. J.; Liu, L.; Luo, Y.; Zhao, H. Y. *Langmuir* **2009**, *25*, 744.
(14) (a) Wang, L. Y.; Yan, R. X.; Hao, Z. Y.; Wang, L.; Zeng, J. H.; Bao, H.; Wang, X.; Peng, Q.; Li, Y. D. *Angew. Chem., Int. Ed.* **2005**, *44*, 6054. (b) Oh, E.; Hong, M. Y.; Lee, D.; Nam, S. H.; Yoon, H. C.; Kim, H. S. *J. Am. Chem. Soc.* **2005**, *127*, 3270. (c) Wang, M.; Hou, W.; Mi, C. C.; Wang, W. X.; Xu, Z. R.; Teng, H. H.; Mao, C. B.; Xu, S. K. *Anal. Chem.* **2009**, *81*, 8783. (d) Wang, L. Y.; Li, Y. D. *Chem.—Eur. J.* **2007**, *13*, 4203.
(15) (a) Wang, F.; Banerjee, D.; Liu, Y.; Chen, X.; Liu, X. *Analyst* **2010**, *135*, 1839. (b) Feng, J.; Shan, G.; Maquieira, A.; Koivunen, M. E.; Guo, B.; Hammock, B. D.; Kennedy, I. M. *Anal. Chem.* **2003**, *75*, 5282.
(16) Goodson, R. J.; Doyle, M. V.; Kaufman, S. E.; Rosenberg, S. *Proc. Natl. Acad. Sci. U.S.A.* **1994**, *91*, 7129.
(17) Wang, L. M.; Liu, Y.; Li, W.; Jiang, X. M.; Ji, Y. L.; Wu, X. C.; Xu, L. G.; Qiu, Y.; Zhao, K.; Wei, T. T.; Li, Y. F.; Zhao, Y. L.; Chen, C. Y. *Nano Lett.* **2011**, *11*, 772.
(18) Zhao, G. X.; Yuan, C.; Bian, C. B.; Hou, X. M.; Shi, X. L.; Ye, X. M.; Huang, Z. X.; Huang, M. D. *Protein Expression Purif.* **2006**, *49*, 71.
(19) Meiser, F.; Cortez, C.; Caruso, F. *Angew. Chem., Int. Ed.* **2004**, *43*, 5954.
(20) Hermanson, G. T., In *Bioconjugate Techniques*, 2nd ed.; Academic Press: New York, 2008; p 915.